Cellular/Molecular

The Spatial Organization of Long-Term Synaptic Plasticity at the Input Stage of Cerebellum

Jonathan Mapelli and Egidio D'Angelo

Department of Cellular and Molecular Physiological and Pharmacological Sciences, University of Pavia and National Institute for the Physics of Matter, I-27100 Pavia, Italy

The spatial organization of long-term synaptic plasticity [long-term potentiation (LTP) and long-term depression (LTD)] is supposed to play a critical role for distributed signal processing in neuronal networks, but its nature remains undetermined in most central circuits. By using multielectrode array recordings, we have reconstructed activation maps of the granular layer in cerebellar slices. LTP and LTD induced by theta-burst stimulation appeared in patches organized in such a way that, on average, LTP was surrounded by LTD. The sign of long-term synaptic plasticity in a given granular layer region was directly correlated with excitation and inversely correlated with inhibition: the most active areas tended to generate LTP, whereas the least active areas tended to generate LTD. Plasticity was almost entirely prevented by application of the NMDA receptor blocker, APV. This suggests that synaptic inhibition, through a control of membrane depolarization, effectively regulates NMDA channel unblock, postsynaptic calcium entry, and the induction of bidirectional synaptic plasticity at the mossy fiber–granule cell relay (Gall et al., 2005). By this mechanism, LTP and LTD could regulate the geometry and contrast of network computations, preprocessing the mossy fiber input to be conveyed to Purkinje cells and molecular layer interneurons.

Key words: **LTP; LTD; synaptic inhibition; cerebellum; granular layer; multielectrode array; signal propagation**

Introduction

There is a strict relationship between synaptic inhibition, long-term synaptic plasticity, and the spatial organization of brain circuit computation. On the one hand, synaptic inhibition limits the intensity, persistence, and spread of excitation in neuronal circuits (von Békésy, 1967; Dudel, 1983; Contreras and Llinas, 2001; Derdikman et al., 2003; Petersen et al., 2003; Wirth and Lüscher, 2004). On the other hand, the inhibitory control of cell depolarization can regulate NMDA channel unblock (Nowak et al., 1984), postsynaptic Ca^{2+} influx, and the induction of synaptic plasticity (Lisman, 2003). Despite the remarkable consequences it might have on neural circuit computation (Kohonen, 1984; Rieke et al., 1997; Singer, 1999), the spatial organization of synaptic plasticity and its inhibitory control are still mostly unknown.

The cerebellum granular layer provides the opportunity for investigating the spatial distribution of long-term synaptic plasticity and its relationship with synaptic inhibition in a relatively simple and well known circuit (Ramon y Cajal, 1911; Eccles et al., 1967). The granule cells are excited by mossy fibers, which branch into clusters distributed in the parasagittal plane (Wu et al., 1999; Sultan, 2001), and are inhibited by Golgi cells. These, in turn, are activated by mossy fibers directly and through the granule cell axon, the parallel fiber. Golgi cell–granule cell neurotransmission is GABAergic (Brickley et al., 1996; Hamann et al., 2002), whereas mossy fiber–granule cell neurotransmission is glutamatergic and develops NMDA receptor-dependent long-term potentiation (LTP) after high-frequency mossy fiber activation (D'Angelo et al., 1999; Armano et al., 2000; Hansel et al., 2001). According to a bidirectional rule, LTP was shown to require stronger granule cell activation than long-term depression (LTD) (Gall et al., 2005). Golgi cell synaptic inhibition, by controlling membrane potential, may thus regulate the induction of synaptic plasticity between mossy fibers and granule cells and, eventually, determine the spatial organization of plasticity in the granular layer.

In this work, the activation pattern after mossy fiber stimulation in the granular layer of acute cerebellar slices was reconstructed by using multielectrode array (MEA) recordings (Egert et al., 2002). After assessing the cellular and circuit mechanism of MEA field potentials, we addressed the relationship between excitation, inhibition, and plasticity. Granule cell activity showed a patchy configuration and its extension was limited by inhibition through the Golgi cell loop, which specifically controlled delayed components of the response and NMDA receptor activation. Granular layer responses were spatially organized so that (1) inhibition was strongest in areas of the granular layer surrounding

Received July 6, 2006; revised Dec. 9, 2006; accepted Dec. 23, 2006.

This work was supported by European Community Grants SPIKEFORCE IST-2001-35271, CEREBELLUM QLG3-CT-2001-02256, and SENSOPAC FP6-IST028056; by FIRB-RBNE01AAS7 (Ministry of Education, University, and Research, and National Institute for the Physics of Matter–Italian National Research Council); and by Fondazione CARIPLO of Italy. We thank Elisabetta Cesana and Lia Forti for their contribution to LCA recordings; Paola Rossi, Lisa Mapelli, Anna D'Errico, and Francesca Prestori for helpful discussion on the inhibitory circuit and bidirectional plasticity; Shyam Diwakar and Segio Solinas for anticipating observations on field potential reconstruction; Bruno Rivieccio for sharing observations *in vivo*; and Daniela Gandolfi for data analysis.

Correspondence should be addressed to Egidio D'Angelo, Department of Cellular and Molecular Physiological and Pharmacological Sciences, University of Pavia and National Institute for the Physics of Matter, Via Forlanini 6, I-27100 Pavia, Italy. E-mail: dangelo@ unipv.it.

DOI:10.1523/JNEUROSCI.4873-06.2007

 0270-6474/07/271285-12$15.00/0

(or adjacent to) the granule cells that were strongly activated by mossy fiber stimulation, (2) when inducing plasticity using theta-burst stimulation (TBS), LTD was more likely in areas that surrounded (or were adjacent to) granule cells undergoing LTP, and (3) the areas receiving strongest inhibition were also the areas more likely to undergo LTD. In this way, LTP and LTD tended to form a Mach-band pattern (von Békésy, 1967), raising the contrast between neighboring areas. The tight relationship between local circuit dynamics and long-term synaptic plasticity complements previous granular layer theories (Eccles, 1969; Marr, 1969; Albus, 1971) and suggests a distributed mechanism for learning and processing spatiotemporal patterns at the input stage of the cerebellum (De Schutter and Bjaalie, 2001; Jorntell and Ekerot, 2002).

Materials and Methods

Extracellular field potentials were recorded from acute cerebellar slices with an MEA. Except for spontaneous activity measured in the Purkinje cell layer (Egert et al., 2002), this is to date the first MEA investigation of the spatial organization of electrical activity evoked in the granular layer *in vitro*.

Slice preparation and maintenance. Acute cerebellar slices (220 μm thick) were obtained from 18- to 25-d-old Wistar rats as reported previously (D'Angelo et al., 1995, 1999). Briefly, rats were anesthetized with Halotane (Sigma, St. Louis, MO; 0.5 ml in 2 L for 1–2 min) before being killed by decapitation. The cerebellum was gently removed, and the vermis was isolated, fixed on a plastic support with cyanoacrylic glue, and immersed into a cold (2−3°C) cutting solution. Slices (220 μm thick) were cut in the sagittal plane. The cutting solution (Dugué et al., 2005) contained the following (in mM): 130 K-gluconate, 15 KCl, 0.2 EGTA, 20 HEPES, 10 glucose, pH 7.4 with NaOH. Slices were incubated for ~1 h before recordings at 31°C in oxygenated Krebs' solution containing the following (in mM): 120 NaCl, 2 KCl, 1.2 $MgSO_4$, 26 $NaHCO_3$, 1.2 KH_2PO_4, 2 $CaCl_2$, 11 glucose, pH 7.4 when equilibrated with 95% O_2–5% CO_2. In certain experiments, the extracellular solution was added with the $GABA_A$ receptor blocker, 10 μM bicuculline (Sigma), the NMDA and AMPA receptor blockers, 50 μM D-APV (Tocris Cookson, Bristol, UK) and 10 μM 6-nitro-7-sulfamoylbenzo(*f*)quinoxaline-2,3-dione (NBQX) (Tocris Cookson). At the end of each experiment, 1 μM TTX (Latoxan, Valence, France) was applied directly into the recording chamber to block synaptic activity and isolate the stimulus artifact.

Slices were gently positioned on the MEA and fixed with a nylon mesh attached to a platinum Ω-wire to improve tissue adhesion and mechanical stability. Perfusion of standard extracellular solution (2–3 ml/min) maintained at 32°C with a feedback temperature controller (Thermostat HC2; Multi Channel Systems, Reutlingen, Germany) was continued during the recording session.

Slices were used soon after incubation to limit potential time-dependent effects deriving from progressive tissue damage. Slices were used soon after incubation to limit potential time-dependent effects deriving from progressive tissue damage. The persistence of spontaneous activity and the stability of granular layer evoked potentials in unperturbed slices (see Fig. 1) indicated constant circuit properties during the course of the experiments. Loose cell-attached (LCA) recordings and whole-cell recordings (WCRs) were performed as reported by Forti et al. (2006) and Nieus et al. (2006), whereas MEA recordings are described in detail below.

MEA recordings. The MEA system consisted of a chip (a silicon substrate supporting thin film platinum wires leading to the electrodes and insulated with a 5-μm-thick SU-8 epoxy layer) connected to amplifiers via printed circuit boards (MEA60; Multi Channel Systems). MEAs contained 60 conic electrodes covered with a thin platinum film arranged in an 8 × 8 matrix (without corner electrodes) and spaced by 100 μm center-to-center (Ayanda Biosystems, Lausanne, Switzerland) (Heuschkel et al., 2002). The electrodes had a base diameter of 40 μm and height of 30 μm, with an effective recording area of 1600 μm^2. The choice of conic electrodes to record from the inner part of the slice was aimed at preventing the effects of fiber discontinuation and neuronal damage occurring on the surface.

MEA signals were amplified (1200×) (MEA1060; Multi Channel Systems) and sampled at 20 kHz/channel. Field potentials usually ranged between tens of microvolts to millivolts. A signal was analyzed only when >10 μV. According to electrophysiological conventions, negative (downward) signals are determined by sink (inward positive) currents indicating membrane excitation.

Two neighboring electrodes laying across the mossy fiber bundle were used for electrical stimulation. Voltage pulses (±2–8 V; 80–100 μs) were applied through an STG1008 stimulator (Multi Channel Systems) triggering the MEA1060 amplifier interface. Mossy fibers were stimulated with single pulses at a frequency of 0.1 Hz. Synaptic plasticity was induced by eight bursts of 10 impulses at 100 Hz, which were repeated every 250 ms (TBS) (D'Angelo et al., 1999).

The signal-to-noise ratio was improved by averaging 10–16 consecutive traces (see Fig. 1). The stimulus artifact was subtracted off-line using average traces obtained in the presence of 0.1 μM TTX, which suppressed any evoked activity. Electrode location was reconstructed using pictures taken at the end of the recording sessions with a digital camera (Canon Powershot G2) installed on the C-mount of the microscope (Olympus BX51WI; 4× objective; Olympus, Tokyo, Japan).

The nature of cerebellar MEA recordings. The spatial resolution of recordings was limited by the distance between MEA electrodes (100 μm). Electrodes like those used in our recordings detect activity generated within a radius of 30 μm (Egert et al., 2002). On the one hand, this prevented cross talk among electrodes in the granular layer, because granule cells have a diameter of ~5 μm and dendrites usually shorter than 30 μm. On the other hand, the discrete sampling of membrane potentials may cause a discontinuous reconstruction of the activity landscape. The effectiveness of the MEA system in reconstructing activity maps of the granular layer was verified by simultaneous recordings with a fast CCD camera (SciMedia, Irvine, CA; MICAM01; 1 kHz acquisition rate; 10 μm effective pixel size) and the voltage-sensitive dye (VSD) Di-4ANEPPS. The main spatial properties revealed by MEA (organization of excitation and inhibition, relative distribution of LTP and LTD) were also observable using VSD (J. Mapelli and E. D'Angelo, manuscript in preparation) (data not shown), indicating that changing spatial resolution from 100 μm (MEA) to ~10 μm (VSD) is not critical for an effective mapping of population activity in the granular layer. This probably reflects the fact that granule cells activate in cohorts: because there are ~100 neighboring granule cells per glomerulus, each one with a diameter of ~5 μm (Harvey and Napper, 1991), the regions of activity can easily range up to several tens of micrometers. The advantage of MEAs over VSD imaging was the higher time resolution needed to distinguish N_{2a} from N_{2b} (see Fig. 1) and detect their amplitude changes, so that parameters relative to excitation, inhibition, and plasticity could be correlated.

The field potential ($V \propto C \int I_m dt$) (Hubbard et al., 1969) depends on the relative surface of the electrogenic elements of the granular layer. The granule cell–Golgi cell ratio is 500:1 for number of cells (Eccles et al., 1967; Harvey and Napper, 1991) and 3:50 for cell surface (cf. Dieudonne, 1998; D'Angelo et al., 1999). This yields a 30 times larger electrogenic surface for granule cells, which therefore determine most of the signal. Indeed, the regular spontaneous activity around 4 Hz typical of Golgi cells appeared in 11 over 498 electrodes. Because ~10% of Golgi cells could be silent (Forti et al., 2006), the effective detection ratio becomes 1:41, in keeping with the surface ratio. When an electrode showed Golgi cell activity, it was discarded from the analysis. The residual probability of having contamination of the field response by the 10% of Golgi cells, which do not show spontaneous discharge but might respond to mossy fiber stimulation, is limited to just 1 of the 498 electrodes (0.2%) analyzed in this study. These observations support previous reports indicating that Golgi cell evoked responses do not substantially contribute to granular layer field potentials in acute rat cerebellar slices (Garthwaite and Brodbelt, 1989; Maffei et al., 2002). Accordingly, the salient properties of the granular layer field potential could be reconstructed using a multicompartmental model of granule cell activity (S. Diwakar and D'Angelo, manuscript in preparation).

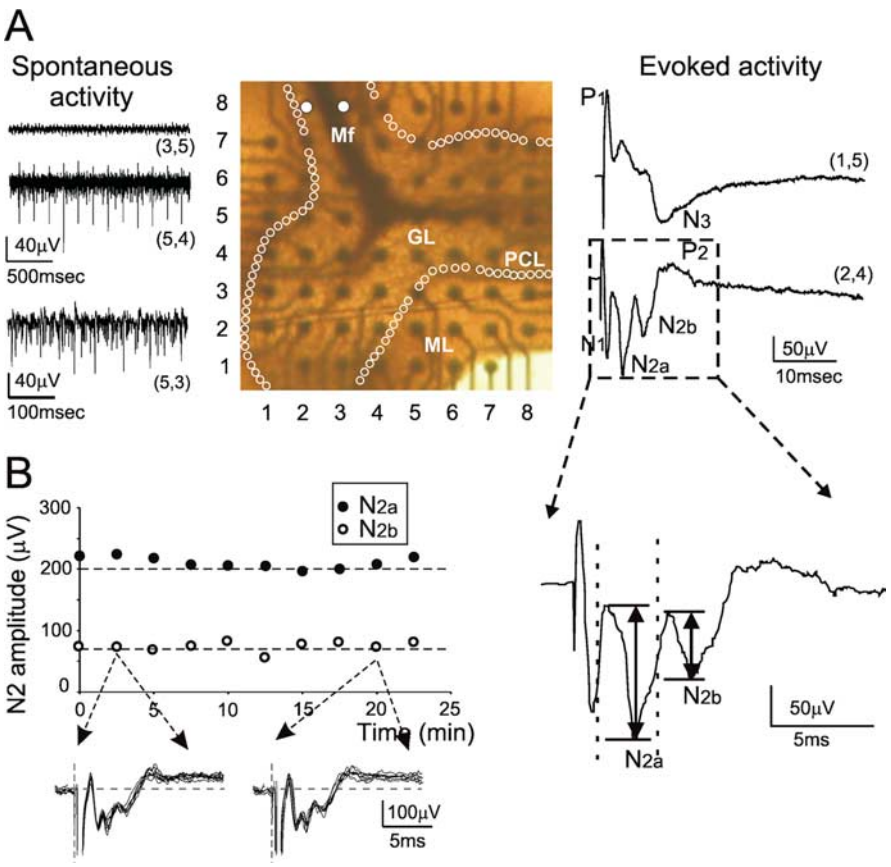

Figure 1. MEA recordings in acute cerebellar slices. ***A***, The picture in the middle shows a parasagittal slice of the cerebellar vermis (thickness, 220 μm) placed on an MEA. Electrodes are indicated by (x, y) coordinates. Mf, Mossy fiber; GL, granular layer; PCL, Purkinje cell layer (white circles); ML, molecular layer. The pair of white dots indicates stimulating electrodes. The left traces show spontaneous activity on different electrodes. The GL is usually silent [electrode (3,5)] except for the occasional observation of low-frequency Golgi cell rhythmic firing [electrode (5,4)]. Spontaneous high-frequency discharge is usually found in the PCL [electrode (5,3)]. The right traces show evoked activity on two different electrodes. The granular layer electrode [electrode (2,4)] shows the typical N_1–N_2–P_2 complex. The molecular layer [electrode (1,5)] shows a wave complex with inverted polarity. Each trace is the average of 10 responses. The stimulus artifact was digitally subtracted using the TTX-trace obtained at the end of the recording (data not shown). The inset shows an enlarged view of the granular layer field response [electrode (2,4)]. The vertical arrows indicate the amplitude of N_{2a} and N_{2b}. ***B***, Time course of N_{2a} and N_{2b} peak amplitude for a granular layer electrode demonstrating recording stability over time. The inset shows individual traces used to measure average amplitudes (the stimulus artifact is partially blanked).

The presence of autorhythmic Golgi cell activity and of appropriate wave sequences in the evoked field response (see Fig. 1) attest to the integrity of the local granular layer circuitry. A finer assessment, which is required to reliably analyze the spatial organization of activity, was obtained by correlating the delay and amplitude of the field responses with distance from the stimulating electrode. If fibers are progressively interrupted, then the furthest responses should be systematically smaller than those recorded in proximity of the stimulating electrode. As shown in the supplemental material (available at www.jneurosci.org), this was not the case: field response amplitude was not correlated with distance (N_{2a} amplitude was 265.6 ± 17.6 μV at <700 μm and 245.5 ± 18.3 μV at >700 μm; $p = 0.43$, paired t test) but rather with peak time delay, which, in turn, depends on the intensity of granule cell activation (see also Figs. 3, 4).

The integrity of slice circuitry was also assessed through independent observations. During MEA experiments, other slices cut from the same preparation were used for patch-clamp recordings from Golgi cells and granule cells. In patch-clamp recordings, ~90% of Golgi cells were autorhythmic (Forti et al., 2006) and almost all of them showed robust synaptic responses and spikes after mossy fiber stimulation (E. Cesana and L. Forti, manuscript in preparation). Moreover, 90% of granule cells ($n = 61$ of 68) showed spontaneous TTX-sensitive IPSCs indicating that they were connected to spontaneously active Golgi cells. From anatomy, it is expected that each granule cell receives two to four Golgi cell inhibitory synaptic contacts on average (Harvey and Napper, 1991). The fact that spontaneous IPSC frequency was two to four times higher than that of individual Golgi cells suggests that the appropriate number of active Golgi cells was connected to granule cells (P. Rossi and L. Mapelli, manuscript in preparation). Finally, LTP and LTD could be induced according to a bidirectional rules based on the intensity of membrane depolarization (A. D'Errico and D'Angelo, manuscript in preparation). We have therefore to conclude that the integrity of local mossy fiber–Golgi cell–granule cell inhibitory circuits in MEA recordings was not substantially altered.

Data analysis. Data were displayed on-line and stored using McRack software (Multi Channel Systems). After off-line digital subtraction of stimulus artifacts, evoked activity recorded from electrodes laying in the granular layer was analyzed using routines written in the IGOR (Wavemetrics, Lake Oswego, OR) and MATLAB (Mathworks, Natick, MA) environment. The intensity of the response was determined by measuring the amplitude of negative peaks, N_1, N_{2a}, and N_{2b} (downward with the present convention) (see Fig. 1). In a defined time window, an automatic procedure detected the local maximum (base) and minimum (peak) yielding the relative peak amplitude (peak-base). This allowed measurement of amplitude, delay, and slope of the waves and reconstruction of their time course along the experiments. To create three-dimensional (3D) maps, the electrode array was represented as an (x, y) matrix and the corresponding amplitude values were plotted on the z-axis. Pseudocolors and spatial interpolation were used to improve the graphics.

A total of 498 electrodes responded to mossy fiber stimulation of 684 electrodes laying in the granular layer (73.4%). These electrodes belonged to 29 slices: with 60 electrodes per slice, 39% of them (~23/slice) were in the granular layer. The multidimensional space governing the geometry of excitation, inhibition, and plasticity poses specific analysis problems, which are briefly summarized here (see also Wirth and Lüscher, 2004). A preliminary analysis of field potentials indicated that the differential behavior of the two wave peaks, N_{2a} and N_{2b}, could be exploited to simultaneously monitor the processes controlling induction and expression of plasticity through the inhibitory loop. At a first stage, statistics of the parameters and their pairwise correlations were analyzed. The excitatory/inhibitory balance (E/I) was introduced to synthetically represent circuit control of granule cell membrane potential. At a further stage, we considered the spatial relationships between parameters by analyzing the geometry of changes in 3D maps. Difference-maps were used to reveal the intensity and spatial distribution of changes (see Fig. 5).

The intensity of synaptic plasticity was estimated by calculating the difference between average amplitude in control and after TBS. Only variations persisting until the end of the recording period were identified as LTP or LTD, whereas those vanishing in 5–10 min were classified as short-term potentiation or short-term depression. To prevent ambiguity in the interpretation of small changes, variations <10% were not considered (see Fig. 10*C*). When analyzing the relative distribution of LTP and LTD, if more than one electrode was potentiated, the analysis was referred to the most potentiated one (see Fig. 9). All data are reported as

mean ± SEM, and, unless otherwise indicated, statistical comparisons were done using paired Student's *t* test.

Results

The spatial organization of synaptic inhibition and plasticity in the cerebellum granular layer was investigated with MEA recordings in acute rat cerebellar slices. Because this technique is not commonly used to record cerebellar activity, we will first consider the fundamental properties of MEA field recordings (Figs. 1–4). This initial analysis will allow definition of the criteria for investigating the spatial organization of synaptic excitation, inhibition, and plasticity.

MEA recordings from the cerebellum granular layer

In MEA recordings, the granular layer was usually silent, reflecting the fact that granule cells do not show any spontaneous activity unless they are stimulated by mossy fibers. However, in some cases, one of the electrodes revealed a regular rhythmic activity at 4.86 ± 0.45 Hz ($n = 11$) reflecting spontaneous discharge in a Golgi cell (Dieudonné, 1998; Forti et al., 2006). Electrodes in the Purkinje cell layer and the molecular layer usually showed single-unit or multiunit activity, with spikes occurring irregularly at relatively high frequency (10–40 Hz). This could be attributable to Purkinje cells (Schonewille et al., 2006) and inhibitory interneurons (Mann-Metzer and Yarom, 2000), which discharge spontaneously in cerebellar slices.

Field potentials were evoked by mossy fiber electrical stimulation (Fig. 1*A*). In the granular layer, field potentials showed the typical N_1–N_2–P_2 complex observed after white-matter cerebellar stimulation *in vivo* (Eccles et al., 1967). At high stimulus intensity, N_2 split into multiple components, the first two of them being named N_{2a} and N_{2b}. Over a large sample (12 slice and 236 electrodes), average peak times for these waves were as follows: N_1, 1.17 ± 0.03 ms; N_{2a}, 2.86 ± 0.02 ms; N_{2b}, 5.05 ± 0.02 ms; P_2, 12.23 ± 1.32 ms. N_1 corresponds to the presynaptic volley and mossy fiber terminal invasion (N_1 was not discernible from the stimulus artifact in some recordings). N_2 is determined by granular layer postsynaptic activity, which is by its most part generated by granule cells, whereas P_2 reportedly corresponds to return currents from the molecular layer and is influenced by local protracted depolarizing currents (Garthwaite and Brodbelt, 1989; Maffei et al., 2002). In the molecular layer, signals often showed

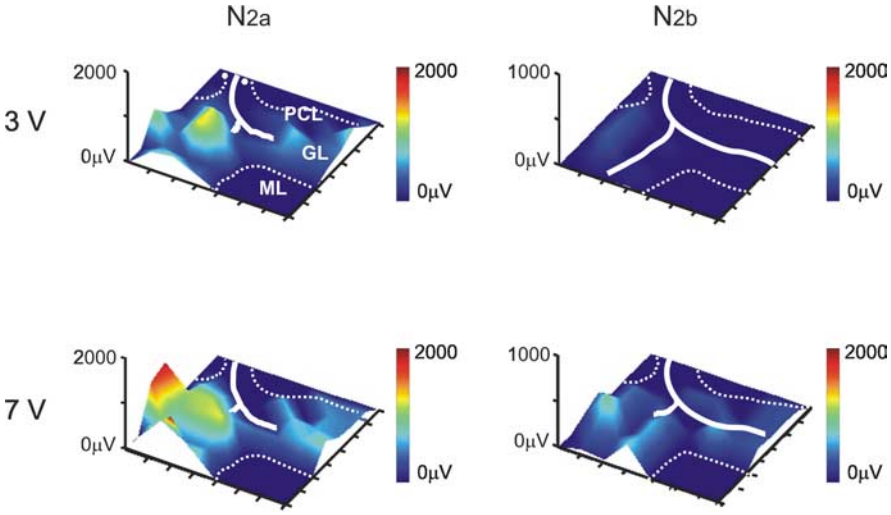

Figure 2. Electrical maps of evoked granular layer activity. Electrical 3D maps for N_{2a} and N_{2b} were constructed from responses to mossy fiber stimulation at two different intensity (3 and 7 V). Pseudocolors improve perception of the vertical dimension. Excitation diffused to both sides of the mossy fiber bundle, revealing patches of activity. Increasing stimulation intensity enhanced the signal. In these and subsequent maps, the granular layer is delimited with thin dashed contours passing over the Purkinje cell layer, and continuous white lines indicate the mossy fiber bundle. Two white dots indicate the stimulation site. Also note that, to complete the graphic matrix, the corner points have been artificially set to 0.

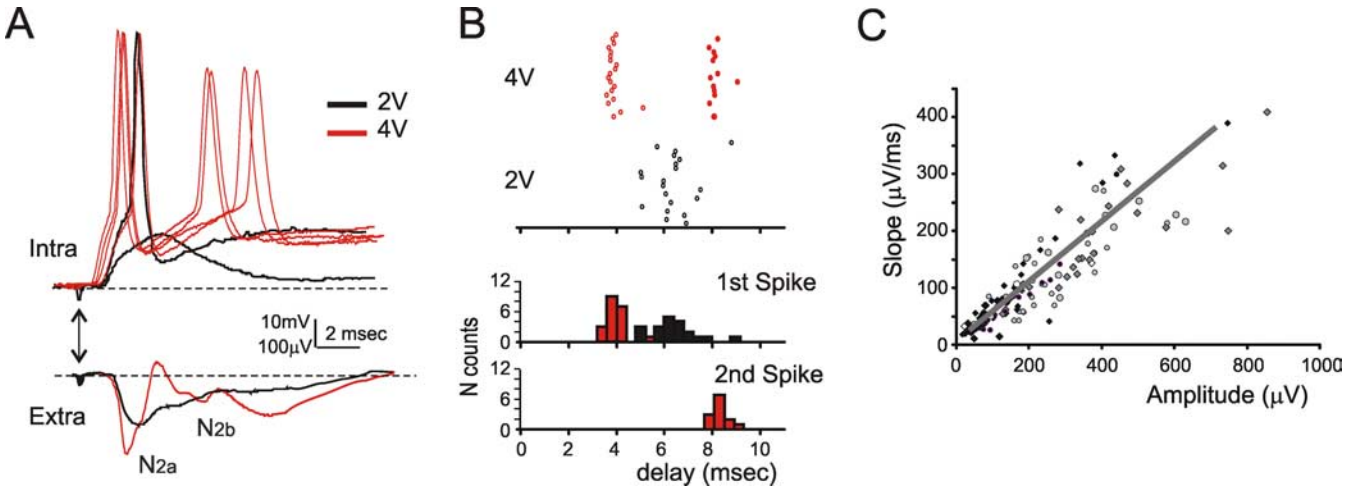

Figure 3. The relationship between field potentials and granule cell activity. ***A***, Signals recorded at high and low stimulation intensity (red and black traces) are compared in the field response (bottom) and in WCRs (top). Several sweeps are shown for the high-intensity intracellular signal to illustrate the variability of the spike generation mechanism (traces show either one or two spikes with variable latency). When stimulus intensity is increased, a spike appears followed by an afterhyperpolarization, and then N_{2a} splits from N_{2b}. Intracellular EPSPs and spikes (single responses) occur in correspondence with the extracellular signals (average of 10 responses). A double arrow indicates the stimulation time. ***B***, Granule cell spikes were recorded in LCA. At low intensity of stimulation, only a delayed spike response is observed (open circles). By raising stimulation intensity, the spike anticipates and becomes more regular. Moreover, a second spike emerges (filled circles). The PSTH shows peaks corresponding to N_{2a} and N_{2b}. The colors indicate different stimulation intensities. ***C***, The plot shows the relationship between peak amplitude and slope for N_{2a} (linear fit, $R^2 = 0.78$; 120 electrodes in 7 slices). The different symbols indicate different slices.

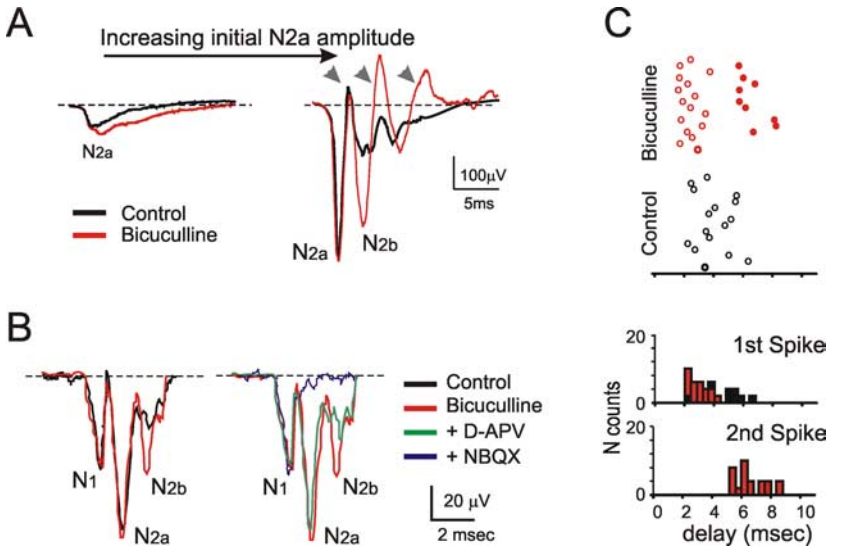

Figure 4. The pharmacology of field potentials. ***A***, Field potentials on a single electrode are reported from a sequential experiment in which, after a control period, drugs were added to the extracellular solution. The control field potentials are modified by application of 10 μM bicuculline. EPSP-like responses show a slow, smooth time course. In spiky responses, N_{2a} peak is left unchanged by bicuculline, but N_{2b} is markedly enhanced and is followed by oscillations, the first of which corresponds to N_{2b}. ***B***, In a different experiment than in ***A***, after application of 10 μM bicuculline, N_{2b} is enhanced. Then, subsequent application of the NMDA receptor blocker, 50 μM D-APV, reduces N_{2b}. Addition of the AMPA receptor blocker, 10 μM NBQX, abolishes the postsynaptic field response. N_1 is left unchanged by these receptor antagonists, confirming its presynaptic nature. Each trace in ***A*** and ***B*** is the average of 10 responses. ***C***, Granule cell spikes were recorded in LCA before and after application of 10 μM bicuculline. In control, a delayed and scattered spike response is observed (open circles). After bicuculline application, the first spike anticipates and a second spike emerges (filled circles). The PSTH shows peaks corresponding to N_{2a} and N_{2b}.

the N_3 wave, which represents responses from Purkinje cells and molecular layer interneurons.

The presence of appropriate spontaneous and evoked activity attests to the integrity of the slice circuitry, as further considered in Materials and Methods and the supplemental material (available at www.jneurosci.org). MEA signals demonstrated a remarkable stability (Fig. 1*B*) and could therefore be used for the analysis of long-term synaptic plasticity in the granular layer circuit.

The spatial distribution of electrical responses in the granular layer after mossy fiber stimulation was reconstructed by generating 3D maps for N_{2a} and N_{2b} (Fig. 2). Usually, activity diffused to both sides of the mossy fiber bundle revealing patches, which formed an irregular landscape with peaks and valleys. By raising stimulation intensity, N_{2a} and N_{2b} activity was enhanced, indicating recruitment of mossy fibers.

Field potentials reveal generation of spike doublets in granule cells

By raising stimulation intensity, N_{2a} changed from an EPSP-like to a spike-like shape and its time of occurrence was anticipated. At the same time, N_{2b} emerged as a second spike-like wave. In experiments in which we paired WCR with field recordings ($n = 3$), we observed that N_2 changes occurred in correspondence with transition from EPSPs to EPSP-spike complexes (Fig. 3*A*) [cf. Maffei et al. (2002), their Fig. 1] and that N_{2b} was indeed related to secondary spikes. This is in keeping with the original observation that granule cells, when sufficiently depolarized, can respond with doublets (or even triplets) of spikes after a single mossy fiber impulse (D'Angelo et al., 1995).

To further clarify the process of N_2 wave generation, we have used LCA recordings (Forti et al., 2006) (Fig. 3*B*). LCA recording prevents changes in resting membrane potential, allowing a direct comparison with MEA extracellular signals. The analysis of poststimulus time histograms (PSTHs) revealed that raising stimulation (from 2 to 4 V) anticipated the first spike (by 2.9 ± 0.37 ms; $n = 3$) and increased the frequency of occurrence of the second spike (from 0 to 71.7 ± 0.5%; $n = 3$; in these recordings, the probability occurrence of the first spike was already saturated at the lowest stimulation intensity).

This observation substantiates the conclusion that spike generation in granule cells is a major determinant of N_{2a} and N_{2b}. The relationship between N_2 waves and synaptic activation of granule cells was clarified by noting that N_{2a} peak amplitude was linearly correlated with the initial slope (Fig. 3*C*), which is proportional to the synaptic current (Hubbard et al., 1969). Thus, on average, the synaptic current and the fraction of granule cells generating suprathreshold activity vary by a similar amount, indicating that N_{2a} amplitude is a good indicator of the strength of synaptic transmission.

The N_{2b} wave is regulated by synaptic inhibition and NMDA receptors

Granule cell activation is regulated by mossy fibers and Golgi cells and therefore by synaptic activation of glutamate and GABA receptors.

The $GABA_A$ receptor antagonist, 10 μM bicuculline, intensified the response by causing specific changes in the field potential waveforms (Fig. 4*A*,*B*). When the response had an EPSP-like shape, it was slightly enhanced by bicuculline (5.02 ± 1.16%; 19 electrodes in seven slices). When the response was spike-like, bicuculline anticipated N_{2a} without changing its amplitude significantly (1.5 ± 2.58%; $n = 7$ slices; $n = 180$ electrodes; $p < 0.51$). However, N_{2b} was markedly enhanced (+309.84 ± 73.5%; $n = 7$ slices; $n = 180$ electrodes; $p < 0.012$) and often further peaks appeared, so that the response resembled an oscillating waveform. The invariance of N_{2a} amplitude with marked N_{2b} changes is consistent with previous observations showing that inhibition reaches its maximum efficiency 3–5 ms after mossy fiber stimulation because of delays in the Golgi cell circuit (Armano et al., 2000), so that the first granule cell spike can arise while the subsequent membrane depolarization and secondary spikes are strongly depressed. Indeed, in LCA recordings (Fig. 4*C*), application of bicuculline did not change the probability of observing the first spike (from 99.3 ± 2.2 to 100%; $n = 3$) but raised the probability of obtaining the second spike considerably (from 0 to 60.4 ± 0.7%; $n = 3$).

After application of bicuculline (Fig. 4*C*), the NMDA receptor antagonist, 50 μM APV, reduced excitation more markedly on N_{2b} than N_{2a} (−40.36 ± 8.29% vs −11.08 ± 5.83%; $n = 5$ slices, $n = 70$ electrodes, with $p < 0.05$ in both cases, which were significantly different from each other at $p < 0.01$, paired t test) confirming the primary role of these receptors in generating delayed components of the mossy fiber–granule cell synaptic response (Garthwaite and Brodbelt, 1989; D'Angelo et al., 1995). Addition of the AMPA receptor antagonist, 10 μM NBQX, fully blocked the postsynaptic response, leaving only the presynaptic volley, N_1.

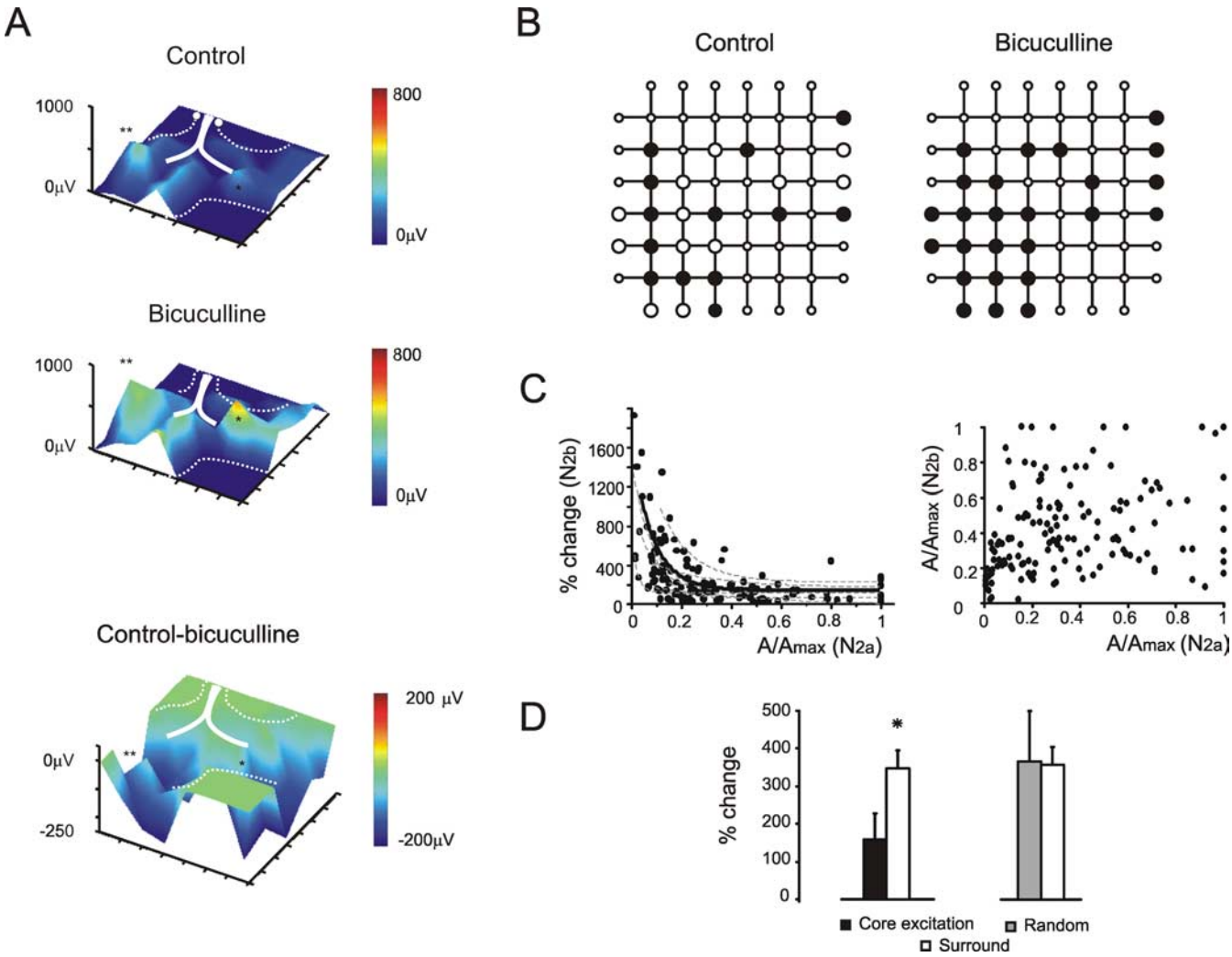

Figure 5. The relationship between excitation and inhibition. ***A***, Electrical 3D maps show N_{2b} amplitude before and after application of 10 μM bicuculline. Bicuculline disinhibited several areas. The distribution and intensity of the inhibitory effect is demonstrated by the subtraction map (control − bicuculline). ***B***, In the same slice shown in ***A***, the number of electrodes measuring a detectable N_{2b} response after bicuculline application (black dots) is increased. Note that N_{2a} was already measurable over the electrodes showing N_{2b} after bicuculline application (large open dots). ***C***, Left, Plot of N_{2b} changes caused by bicuculline as a function of N_{2a} amplitude. The plot reveals a strong negative correlation between the parameters. The thick line is a monoexponential fitting to the whole dataset [$y = y_0 + A \times \exp(-x/\tau)$, with $y_0 = 95$, $x_0 = 0$, $A = 1174$, $\tau = 0.09$; $p(\chi^2) < 0.001$; $R^2 = 0.72$; $n = 180$ in 7 slices], the thin dashed lines are fittings to single-slice data (always $R^2 > 0.6$). Right, Plot of N_{2b} versus N_{2a} initial amplitude from the same slices: note the absence of correlation. For each slice, N_{2a} and N_{2b} amplitudes are normalized to their maximum control value. ***D***, The histogram shows the average change caused by bicuculline in the electrodes with a local peak of excitation versus the surrounding ones. The effect of bicuculline is stronger in the surround ($n = 60$ from 7 slices; $^*p < 0.03$, paired t test). No comparable difference is observed by random sampling the granular layer electrodes and measuring the surrounding activity ($n = 60$ from 7 slices; $p = 0.74$, paired t test). Error bars indicate SEM.

Thus, N_{2a} provides a measure of granule cell excitation almost unaffected by GABAergic inhibition. Conversely, N_{2b} allows evaluation of the effect of GABAergic inhibition and its control over NMDA channel activation. These properties provide the key to correlate excitation, inhibition, and plasticity in granular layer responses. The principles governing the differential contribution of phasic and tonic inhibition (Brickley et al., 1996; Hamann et al., 2002) and NMDA receptors in regulating the granule cell response are considered in the supplemental material (available at www.jneurosci.org).

Synaptic inhibition regulates the intensity and extension of the granular layer response

Although the mechanisms of GABAergic transmission at the Golgi cell–granule cell synapse have been clarified to a considerable extent (Brickley et al., 1996; Hamann et al., 2002), the spatial properties of inhibition are unknown. These were investigated by measuring the N_{2b} changes after application of 10 μM bicuculline and by generating subtraction maps (control − bicuculline) (Fig. 5*A*). Two effects were worth noting. First, bicuculline increased the active surface by 45.9 ± 24.8% ($n = 7$ slices; $n = 180$ electrodes) (Fig. 5*B*). The emergence of N_{2b} in new slice regions indicates that, although these received mossy fiber activation, synaptic inhibition prevented doublet generation (compare Fig. 4). Second, there was a marked negative correlation between initial excitation intensity measured on N_{2a} and the change caused by bicuculline on N_{2b} ($n = 7$ slices; $n = 180$ electrodes; $R^2 = 0.72$; $p(\chi^2) < 0.001$) (Fig. 5*C*). No correlation emerged when initial N_{2a} and N_{2b} amplitudes were compared, supporting the specificity of N_{2b} regulation by the inhibitory circuit.

The negative correlation between excitation and inhibition suggests that inhibition is stronger beside the most excited regions. This hypothesis was tested by analyzing the intensity of inhibition in the electrodes surrounding peaks of excitation (Fig. 5*D*). Inhibition was more intense around peaks than on top of them ($p < 0.03$; $n = 60$ electrodes in 7 slices; paired t test). This

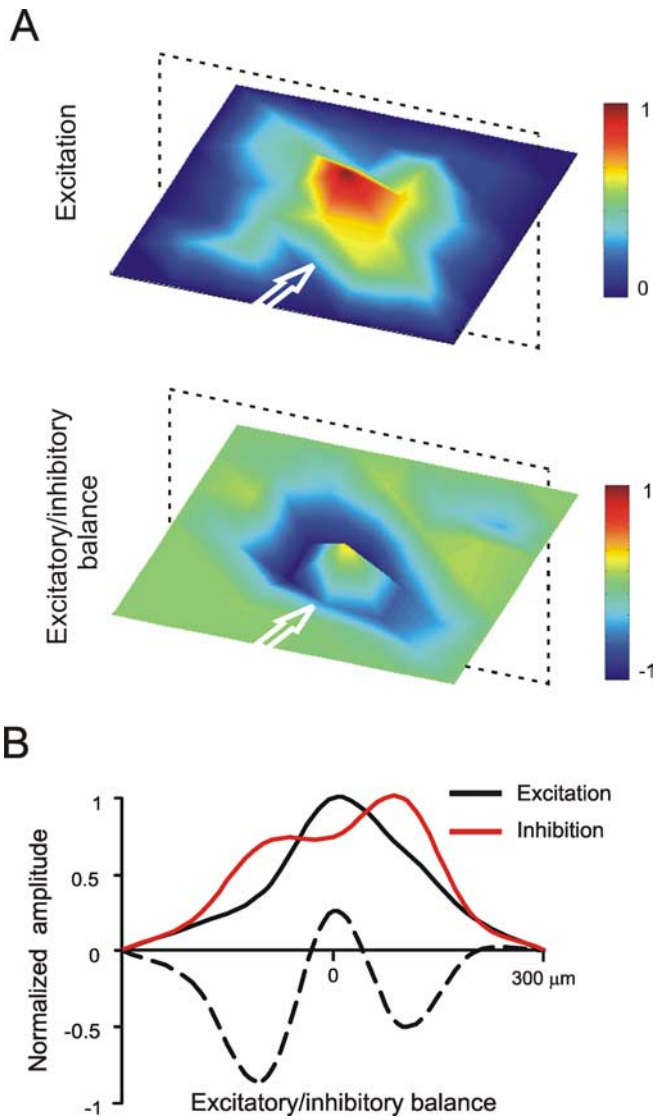

Figure 6. The spatial organization of the excitatory/inhibitory balance. ***A***, The top panel shows an average excitation map (measured from N_{2a}) obtained from seven MEA recordings and 156 electrodes by centering over the highest responses and aligning the corresponding slices along the mossy fiber bundle. To visualize the excitatory/inhibitory balance, we first measured the variation of N_{2b} after bicuculline perfusion, obtaining an inhibition map (data not shown). Then, the inhibition map was subtracted from and normalized to the corresponding excitation map according to the *E*/*I* definition reported in Results. ***B***, The cross section reveals a bell-shaped profile (black line) for excitation. When synaptic inhibition is blocked by bicuculline (red line), the profile broadens and shows depression in the center. The excitatory/inhibitory balance (see definition given above) reveals lateral inhibition (dotted line).

effect did not emerge when the reference electrodes, rather than corresponding to excitation peaks, were chosen randomly in the granular layer ($p = 0.74$; $n = 60$ electrodes in 7 slices; paired t test). This result indicates the presence of a lateral component of inhibition.

The spatial organization of the excitatory/inhibitory balance

To represent the combined effect of excitation and inhibition in controlling local granular layer activity, we have introduced the excitatory/inhibitory (E/I) balance, $E/I = [(E_{norm} - I_{norm})/E_{norm}]$, where E_{norm} and I_{norm} are excitation and inhibition normalized by the maximum value measured in each recording. The spatial organization of the E/I balance was visualized by taking the average of several experiments, in which the slices were centered on the most active electrode and aligned along the mossy fiber axis (Fig. 6). Inhibition was proportionately stronger in the periphery than in the center of the activated area, as evidenced both in the 3D map and in its cross section, resembling distributions observed previously in the CNS (von Békésy, 1967; Dudel, 1983; Contreras and Llinas, 2001; Derdikman et al., 2003; Petersen et al., 2003; Wirth and Lüscher, 2004). At a closer inspection, the spatial profile of excitation (evaluated as N_{2a} amplitude) was bell-shaped, whereas the intensity of inhibition (evaluated as N_{2b} variation after bicuculline) was broader than excitation and showed a depression in the center. It must be noted that the smooth appearance of average maps indicates the absence of any preferential orientation in the inhibitory balance (or plasticity in Fig. 8) relative to the mossy fiber bundle rather than suggesting a symmetric arrangement of the circuit. In other words, the average map smears the fragmentation of patterns observed in individual maps, similar to a filter smoothing a noisy recording.

Multiple sites of origin of LTP and LTD in the granular layer

Long-term plasticity can be induced at the cerebellar mossy fiber–granule cell synapse by TBS (D'Angelo et al., 1999). In these experiments, we have posed two main questions: (1) how are LTP and LTD spatially organized? and (2) how do they relate to excitatory and inhibitory activity?

In MEA recordings, TBS induced either LTP or LTD in different slice regions (Fig. 7*A*) with a time course (Fig. 7*B*) resembling that observed in extracellular focal recordings (Maffei et al., 2002) and in whole-cell recordings from granule cells (Gall et al., 2005). LTP and LTD coexisted in 15 of the 16 slices tested, whereas in one slice recorded without bicuculline only LTD was observed. In control solution, LTD mostly outnumbered LTP electrodes (38 vs 9%; 132 electrodes in seven slices), whereas the opposite happened in the presence of 10 μM bicuculline (19 vs 11%; 140 electrodes in nine slices), indicating a major role of inhibition in regulating plasticity (Fig. 7*A*, histograms). When the preparation was perfused with 50 μM APV, long-term plasticity almost entirely disappeared, indicating its NMDA receptor dependence. Just in a minor number of electrodes (<10%), LTD could still be revealed. On average (Fig. 7*C*), by considering the electrodes showing activity changes >10% over 30 min, in control conditions LTP attained 41 ± 16% ($n = 4$ slices; $n = 12$ electrodes; $p < 4 \times 10^{-8}$) and LTD −59 ± 5% ($n = 4$ slices; $n = 50$ electrodes; $p < 2 \times 10^{-12}$). In the presence of 10 μM bicuculline, LTP attained 40 ± 11% ($n = 7$ slices; $n = 26$ electrodes; $p < 7 \times 10^{-11}$) and LTD –39 ± 8% ($n = 7$ slices; $n = 16$ electrodes; $p < 1 \times 10^{-11}$). Despite their different frequency of occurrence, the intensity and time course of LTP and LTD were similar in the two induction conditions.

Visual inspection of plasticity maps suggests that LTP and LTD tend to appear in neighboring areas. A quantitative analysis of this effect was performed by analyzing plastic changes in the area surrounding LTP (Fig. 7*D*). After TBS, the N_{2a} change averaged over all of the granular layer electrodes next to a potentiated one was negative, revealing a prevalence of LTD ($p < 10^{-5}$; $n = 24$ electrodes in six slices; paired t test). This happened because the electrodes surrounding the one doing LTP showed either LTD or no changes. This effect did not emerge when the reference electrodes, rather than being those showing LTP, were chosen randomly in the granular layer ($n = 34$ from six slices; $p = 0.96$, paired t test). Therefore, the arrangement of LTD beside or around LTP is not a random effect but rather reflects a specific circuit organization.

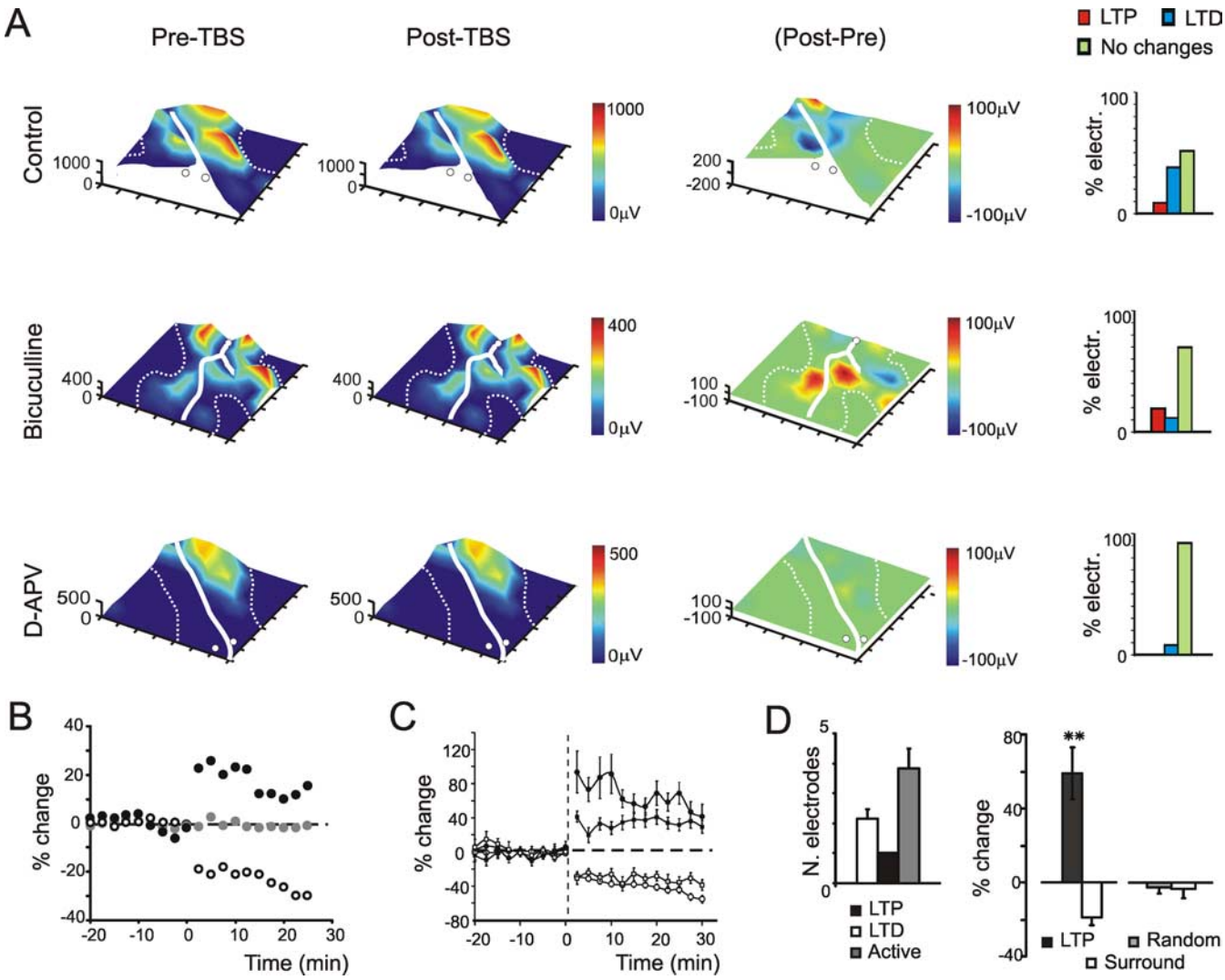

Figure 7. Long-term synaptic plasticity. ***A***, Electrical 3D maps for N_{2a} amplitude were obtained before (Pre-TBS) and after (Post-TBS) application of a TBS in three different solutions (control, bicuculline, APV). The subtraction map (Post–Pre) reveals the localization of LTP (red) and LTD (blue). The histograms at the right indicate the percentage of electrodes generating either LTP, LTD, or no change. After TBS delivered in control extracellular solution, LTD prevails over LTP. After TBS delivered in the presence of 10 μM bicuculline, LTP prevails over LTD. After TBS delivered in the presence of 50 μM [SCAP]D-APV, no remarkable LTP or LTD changes are observed except for a minor occurrence of LTD. The experiments reported in this figure are different from those reported in Figure 4. ***B***, The time course of N_{2a} amplitude changes in control extracellular solution on single electrodes, one showing LTP, one showing LTD, and one showing no long-term plasticity changes [data corresponding to electrodes (2,1), (3,4), and (6,4) in the top right panel of Fig. 6]. ***C***, Time course of N_{2a} amplitude changes in control extracellular solution (circles) and in presence of 10 μM bicuculline (square). The measures were obtained from electrodes showing either positive or negative response variations >10% after TBS (control: $n = 50$ electrodes for LTD, $n = 12$ electrodes for LTP, data from 4 slices; bicuculline: $n = 16$ electrodes for LTD, $n = 26$ electrodes for LTP, data from 7 slices). ***D***, The left histogram shows that around the LTP electrode, there are on average 3.8 $\pm$ 0.7 active granular layer electrodes, 2.2 $\pm$ 0.3 of which showing LTD ($n = 28$ from 6 slices). The right histogram shows the average change in the electrodes surrounding the one with maximal LTP. The net change around the LTP electrode is a significant LTD ($n = 28$ from 6 slices; $^{**}p < 10^{-5}$, paired *t* test). No comparable changes are observed by randomly sampling the granular layer electrodes and measuring the surrounding activity ($n = 34$ from 6 slices; $p = 0.96$, paired *t* test). Error bars indicate SEM.

The spatial organization of synaptic plasticity

Similar to Figure 6, the spatial organization of synaptic plasticity was visualized by centering plasticity maps (evaluated as N_{2a} amplitude) on the electrodes showing maximal LTP and aligning the maps along the mossy fiber axis (Fig. 8). The spatial profile of plasticity resembled a Mexican hat with LTP regions surrounded by LTD. When synaptic inhibition was blocked by bicuculline, the distribution became bell-shaped. By comparing the average maps in Figures 6 and 8, a clear matching emerges between the spatial organization of the *E*/*I* balance and that of LTP and LTD, suggesting that lateral inhibition could provide the organizing principle for the geometry of synaptic plasticity (see below and Discussion).

The relationship between excitation, inhibition, and plasticity

The induction of long-term plasticity in mossy fiber–granule cell synapses is regulated by the intensity of postsynaptic excitation during mossy fiber activity (Gall et al., 2005). We investigated therefore whether plasticity in the present recordings was correlated with N_{2a} amplitude. Plasticity showed a biphasic behavior, with LTD at low and LTP at high N_{2a} amplitude (Fig. 9*A*,*B*). The switch between LTP and LTD was extrapolated from a biexponential fitting to the data and felt at intermediate levels of N_{2a} amplitude. The easier transition from LTD to LTP obtained in the presence of bicuculline indicates that removing inhibition allows for a stronger activation of the induction mechanisms. It should also be noted that a group of electrodes showed LTP at low

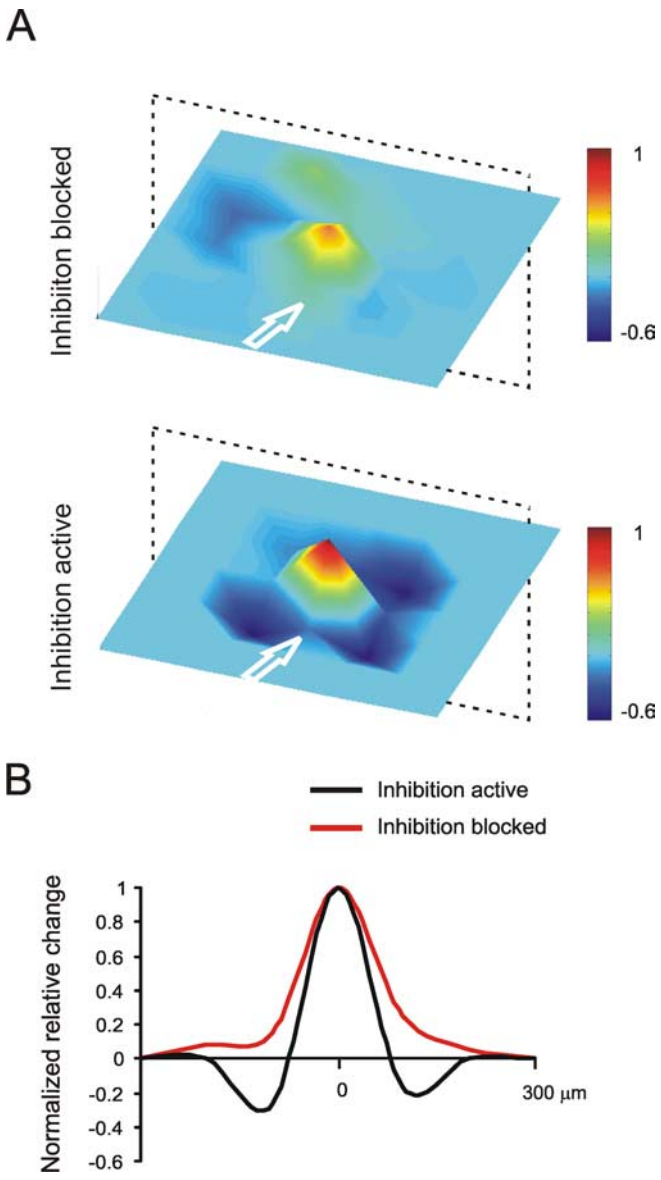

Figure 8. The spatial organization of synaptic plasticity. ***A***, Average plasticity maps are generated from five experiments (62 electrodes) performed in the presence of bicuculline by centering over the electrodes showing maximal LTP and aligning the slices along the mossy fiber bundle (top panel). The averaging procedure was repeated for four MEA experiments and 38 electrodes in control solution (bottom panel). LTP emerges as a red-tipped cone surrounded by a blue ring of LTD, which is almost absent with bicuculline in the bath. ***B***, The cross section reveals a Mexican-hat profile (black line). When synaptic inhibition is blocked by bicuculline (red line), LTD tends to disappear. Note that, because the 3D maps in ***A*** and ***B*** are rather symmetric, the cross section in a plane (indicated by a dotted frame) is representative of the average map profile.

N_{2a} amplitude (Fig. 9*A*,*B*, circled regions), possibly corresponding to synapses with low initial release probability (Sola et al., 2004).

The induction of long-term plasticity in mossy fiber–granule cell synapses is regulated by GABAergic inhibition (Armano et al., 2000; Maffei et al., 2002). To understand the spatial distribution of this action, 30 min after TBS 10 μM bicuculline was perfused to uncover the inhibited regions. Inhibition was stronger in regions generating LTD than in those generating LTP (Fig. 10*A*). The quantitative analysis of field response changes in six MEA recordings (Fig. 10*B*) showed indeed a negative correlation between the change in field responses caused by TBS and the change after bicuculline. To rule out the possibility that changes in synaptic inhibition occurred after TBS, we measured the intensity of inhibition before TBS application (in this protocol, 10 μM bicuculline was applied in control and subsequently washed out: TBS was applied after field potentials recovered their original amplitude; $n = 4$). Also in this case, less inhibited regions potentiated better with a negative correlation between synaptic plasticity and inhibition (Fig. 10*B*).

To represent the combined effect of excitation and inhibition in controlling the induction of synaptic plasticity, we have used the excitatory/inhibitory balance, *E*/*I* (see definition above). In this graph (Fig. 10*C*), for negative *E*/*I* values (inhibition favored against excitation) LTD is the only plasticity observed. For positive *E*/*I* values (excitation favored against inhibition), both LTP and LTD are observed. The presence of LTD in the positive *E*/*I* region is not surprising considering that a positive *E*/*I* does not imply that excitation will pass the threshold for LTP induction: a favorable *E*/*I* may occur with low absolute depolarization or high initial release probability, moving the system toward LTD (compare also Fig. 9).

Discussion

In this paper, by using MEA recording techniques, we investigated the spatial organization of electrical activity in acute rat cerebellar slices after mossy fiber stimulation. We show that the geometry of excitation and inhibition, by controlling a bidirectional mechanism mostly based on NMDA receptor activation, is a key determinant of the sign and distribution of long-term synaptic plasticity. In particular, (1) inhibition was strongest in areas of the granular layer surrounding (or adjacent to) the granule cells that were strongly activated by mossy fiber stimulation; (2) when inducing plasticity using TBS, LTD was more likely in areas that surrounded (or were adjacent to) granule cells undergoing LTP; (3) the areas receiving strongest inhibition were also the areas more likely to undergo LTD. LTP and LTD emerge therefore as distributed network properties with a Mach-band organization (von Békésy, 1967), implying a role in regulating the contrast of network computation.

MEA recordings proved an efficient tool for measuring electrical activity in acute slices, allowing to reconstruct the fundamental aspects of evoked discharge characterizing the cerebellar cortical layers [for the original reports on circuit organization, see Eccles et al. (1967); for granule cells, D'Angelo et al. (1995); for Golgi cells, Dieudonné (1998) and Forti et al. (2006); for Purkinje cell and molecular layer interneurons, Mann-Metzer and Yarom (2000) and Schonewille et al. (2006)]. The evoked granular layer response appeared fragmented and partially surrounded by regions of lateral inhibition. The multiple patches of activity resemble the branching of mossy fibers revealed in the sagittal plane of cerebellar sections (Wu et al., 1999; Sultan, 2001) and may contribute to generate the fractured somatotopy revealed by granular layer micromapping *in vivo* (Shambes et al., 1978). We cannot, however, exclude that, if some mossy or Golgi cell axon fibers were cut at the slice edges, the real geometry would approach a more homogeneous Mexican-hat shape like that emerging from average map analysis.

Granular layer field potentials reflected the generation of granule cell EPSP and EPSP-spike complexes. The presence of multiple peaks (like N_{2a} and N_{2b} as the first two of them) indicated that granule cells can respond to single stimuli with short bursts of spikes, typically doublets (D'Angelo et al., 1995). Although several factors may concur (like spillover on AMPA receptors or activation of a persistent sodium current) (Mitchell

and Silver, 2003; Nieus et al., 2006), doublets were related to an NMDA receptor-dependent depolarization, consistent with early reports suggesting that these receptors enhance the late component of the response (Garthwaite and Brodbelt, 1989; Maffei et al., 2002). Moreover, whereas N_{2a} was uninfluenced, N_{2b} was strongly and specifically reduced by $GABA_A$ receptor activation. Through this delayed action, Golgi cell inhibition can limit the duration of granule cell discharge controlling NMDA channel unblock and the induction of long-term synaptic plasticity. Once plasticity has been induced, N_{2a} can express plasticity through a potentiation mostly mediated by the AMPA receptor response (D'Angelo et al., 1999; Gall et al., 2005).

The action of inhibition was related to activation of the Golgi cell circuit. In previous extracellular recordings [Maffei et al. (2002), their Fig. 1*D*], ~70% of the granule cell response induced by mossy fiber stimulation could be inhibited by an independent Golgi cell stimulation. In addition, tonic inhibition (Brickley et al., 1996; Hamann et al., 2002; Mitchell and Silver, 2003) could promote N_{2b} reduction by accelerating membrane potential relaxation and preventing NMDA channel unblock. Details on the principles governing the action of phasic and tonic inhibition are given in the supplemental material (available at www.jneurosci.org).

Synaptic inhibition limited the excited area resembling observations reported in other brain regions like the cerebral cortex (Contreras and Llinas, 2001; Derdikman et al., 2003; Petersen et al., 2003; Wirth and Lüscher, 2004). The mechanism of lateral inhibition was suggested by the fact that the areas receiving more excitation were also those that were less inhibited. Thus, probably, strongly excited neurons inhibit the neighbors more effectively than weakly excited ones (von Békésy, 1967; Dudel, 1983). The balance between granule cell excitation and inhibition could be sharpened by glomerular cross talk through neurotransmitter spillover, in which GABA presynaptically inhibits glutamate release and vice versa: for instance, strongly excited mossy fibers would prevent GABA release (Mitchell and Silver, 2000a) and limit its depressing action on glutamate release, thereby favoring granule cell excitation (Mitchell and Silver, 2000b). Moreover, the Golgi cell axonal projections extend beyond the input field in basal dendrites [Eccles et al. (1967), their Fig. 19 from Ramon y Cajal (1911)], providing a structural substrate to the lateral inhibition mechanism. Finally, it should be noted that, *in vivo*, Golgi cell receptive fields are wider and in part distinct from those of granule cells (Vos et al., 1999; Jorntell and Ekerot, 2002). Thus, in a natural context, granule and Golgi cell activity should be regulated not only by local circuit organization but also by the topography of the afferent sensory inputs.

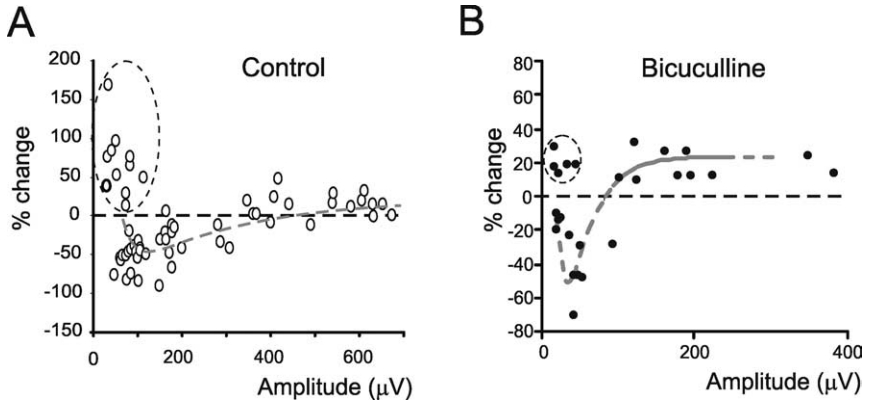

Figure 9. The relationship between plasticity and excitation (***A***). The plot shows the relationship between the relative change during long-term synaptic plasticity and excitation measured as N_{2a} control amplitude. The data shown in this panel were obtained from the electrodes displaying significant N_{2a} changes after TBS, as in ***B***. Note that, for small N_{2a} amplitudes, the electrodes usually show LTD, whereas at large amplitudes they tend to show LTP. The data are interpolated with a double exponential equation [$y = y_0 + A_1 \times \exp(-(x - x_0)/\tau_1) + A_2 \times \exp(-(x - x_0)/\tau_2)$, with $y_0 = 29.5, x_0 = 45.13, A_1 = 99.5, \tau_1 = 24.1, A_2 = -93$, and $\tau_2 = 266$; $n = 62$ electrodes from 4 slices; $p(\chi^2) < 0.01$]. Note also that, in the very low amplitude region, some data points (enclosed in a dashed circle) show LTP. These data have not been used for fitting. ***B***, Same as in ***A***, but in the presence of 10 μM bicuculline [double exponential fitting with $y_0 = 23.5, x_0 = -12, A_1 = 3354, \tau_1 = 9.65, A_2 = -450$, and $\tau_2 = 31.1$; $n = 42$ electrodes from 7 slices; $p(\chi^2) < 0.01$].

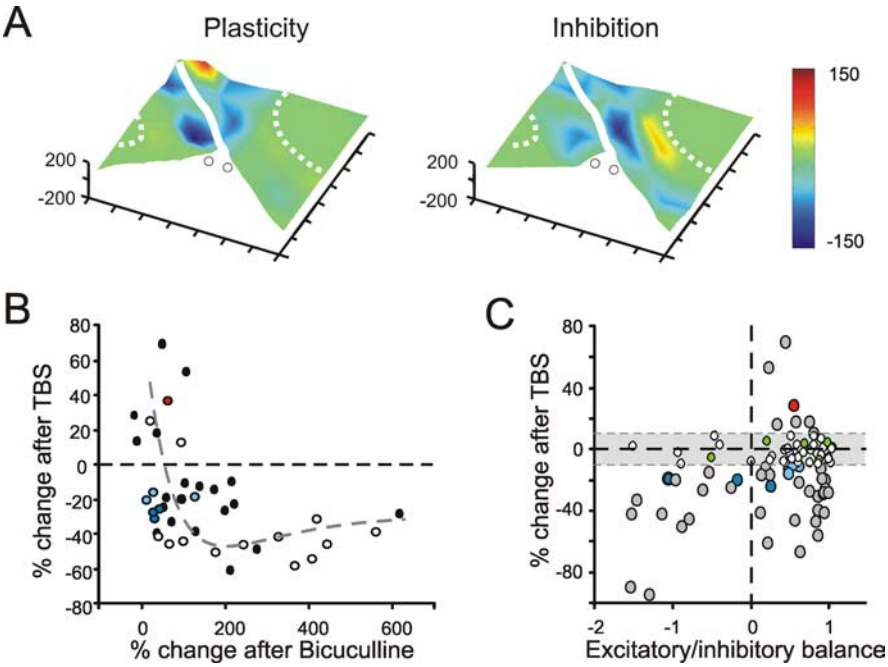

Figure 10. The relationship between plasticity and inhibition. ***A***, The electrical 3D maps compare distribution of plasticity and inhibition. After a control period, synaptic plasticity was induced with TBS. Then, after allowing plasticity to attain a steady level (30 min), 10 μM bicuculline was perfused. It was therefore possible to obtain a plasticity map (post-TBS − control) and the corresponding inhibition map (post-TBS − bicuculline) in the same MEA recording experiment. ***B***, The plot shows the relationship between synaptic plasticity and inhibition for MEA recordings in which inhibition was evaluated after TBS (closed circles; $n = 4$ MEA recordings, $n = 23$ electrodes) (e.g., see ***A***) or before TBS (open circles; $n = 4$ MEA recordings, $n = 22$ electrodes). The colored points code plasticity for the slice shown in ***A***. LTP prevails with little inhibition, LTD with large inhibition. The dotted line is a biexponential fitting to the data [$y_0 = -25, x_0 = 0, A_1 = 142.15, \tau_1 = 90, A_2 = -100, \tau_2 = 160$; $p(\chi^2) < 0.01$]. ***C***, The plot shows the relationship between synaptic plasticity and the excitatory/inhibitory balance (E/I) (definition in the text) for the same recordings used in ***B***. Whereas LTP occurs only at high E/I, LTD occurs at all values. The colored points code plasticity for the slice shown in ***A***. To complete the dataset representation, the white dots show results recorded within the plasticity rejection threshold (less than ±10% change).

The sign of long-term synaptic plasticity in a given granular layer region was directly correlated with excitation and inversely correlated with inhibition: the most excited areas tended to generate LTP, whereas the least excited areas tended to generate LTD. The relationship between synaptic plasticity and local circuit activity was bidirectional, and several recording sites did not show net LTP or LTD. This could be attributable either to the absence of changes in the underlying synapses or to elision of changes with opposite sign. This ambiguity could not be resolved with the present technique, which reveals the average behavior of the local neuronal population. It should also be noted that the excitatory/inhibitory balance may not be the only mechanism of LTP/LTD regulation. For instance, synapses with very low release probability are biased toward LTP (Sola et al., 2004). This may explain the cases of LTP appearing in fields with low response amplitude.

TBS-induced LTP and LTD depended on NMDA receptor activation (except for an exception commented below). Thus, we hypothesize that NMDA receptor-dependent LTP and LTD generated by TBS are two aspects of the same induction mechanism. Supposedly, the intracellular Ca^{2+} increase regulated by NMDA receptors in granule cells is the discriminating factor (Lisman, 2003; Gall et al., 2005). The marked prevalence of LTD in the inhibited areas supports a voltage-dependent switch based on the limitation imposed by GABAergic inhibition on NMDA channel unblock. A residual fraction of LTD (<10% of cases) could still be induced while NMDA receptors were blocked: this may involve voltage-dependent calcium channels or metabotropic glutamate receptors, or simply reflect incomplete block of NMDA receptors in deep slice regions, allowing for a moderate calcium influx and LTD induction. The close correlation of plasticity with the granule cell excitatory/inhibitory balance reinforces the conclusion that changes at the mossy fiber–granule cell relay are the main responsible of the changes caused by TBS.

According to Marr (1969), if input trains saturate granular layer plasticity, this would be inefficient for controlling information processing. Here, we show, however, that TBS did not saturate plasticity but, instead, simultaneously generated LTP and LTD in neighboring granular layer areas. The circuit maintains therefore a sort of homeostatic balance, in which activity is enhanced in certain areas but is reduced in others. Once established, LTP and LTD may be instrumental in regulating the contrast between granular layer fields, extending the original concept of spatial pattern separation (Marr, 1969), in which the excitatory/inhibitory balance of granule cells was predetermined and unchangeable. The LTP and LTD areas may represent channels for differential processing of mossy fiber inputs. In the LTP channel, the delay is reduced and the average frequency of granule cell discharge is enhanced, whereas the opposite happens in the LTD channel (Nieus et al., 2006). By doing so, the LTP (or LTD) channels could favor (or prevent) the activation of specific Purkinje cell and molecular layer interneuron assemblies (Bower, 2002; Lu et al., 2005) as well as the development of short-term (Isope and Barbour, 2002; Sims and Hartell, 2005) and long-term synaptic plasticity (Hansel et al., 2001; Casado et al., 2002) at the corresponding parallel fiber synapses.

Contrast enhancement in the granular layer and Purkinje cell selection may contribute to the spatiotemporal recoding of mossy fiber information predicted by theoretical network analysis (Eccles, 1969; Medina and Mauk, 2000; De Schutter and Bjaalie, 2001) and may take part to cerebellar receptive field reshaping after sensory stimulation (Jorntell and Ekerot, 2002). Artificial network models indicate that combining lateral inhibition with Hebbian learning regulates competition between neighboring areas causing the emergence of self-organized topology, feature abstraction, and generalization (Kohonen, 1984; Rieke et al., 1997; Singer, 1999). Appropriate network simulations may help understanding the potential occurrence of these properties in the granular layer of cerebellum.

References

Albus JS (1971) A theory of cerebellar function. Math Biosci 10:15–61.

Armano S, Rossi P, Taglietti V, D'Angelo E (2000) Long-term potentiation of intrinsic excitability at the mossy fibre–granule cell synapse of rat cerebellum. J Neurosci 20:5208–5216.

Bower JM (2002) The organization of cerebellar cortical circuitry revisited: implications for function. Ann NY Acad Sci 978:135–155.

Brickley SG, Cull-Candy SG, Farrant M (1996) Development of a tonic form of synaptic inhibition in rat cerebellar granule cells resulting from persistent activation of GABAA receptors. J Physiol (Lond) 497:753–759.

Casado M, Isope P, Ascher P (2002) Involvement of presynaptic *N*-methyl-D-aspartate receptors in cerebellar long-term depression. Neuron 33:123–130.

Contreras D, Llinas R (2001) Voltage-sensitive dye imaging of neocortical spatiotemporal dynamics to afferent activation frequency. J Neurosci 21:9403–9413.

D'Angelo E, De Filippi G, Rossi P, Taglietti V (1995) Synaptic excitation of individual rat cerebellar granule cells in situ: evidence for the role of NMDA receptors. J Physiol (Lond) 484:397–413.

D'Angelo E, Rossi P, Armano S, Taglietti V (1999) Evidence for NMDA and mGlu receptor-dependent long-term potentiation of mossy fiber–granule cell transmission in rat cerebellum. J Neurophysiol 81:277–287.

Derdikman D, Hildesheim R, Ahissar E, Arieli A, Grinvald A (2003) Imaging spatiotemporal dynamics of surround inhibition in the barrels somatosensory cortex. J Neurosci 23:3100–3105.

De Schutter ED, Bjaalie JG (2001) Coding in the granular layer of the cerebellum. Prog Brain Res 130:279–296.

Dieudonné S (1998) Submillisecond kinetics and low efficacy of parallel fibre-Golgi cell synaptic currents in the rat cerebellum. J Physiol (Lond) 510:845–866.

Dudel J (1983) General sensory physiology. In: Human physiology (Schmidt RT, Thews G, eds), pp 177–192. Berlin: Springer.

Dugué GP, Dumoulin A, Triller A, Dieudonné S (2005) Target-dependent use of coreleased inhibitory transmitters at central synapses. J Neurosci 25:6490–6498.

Eccles JC (1969) The cerebellum as a computer: patterns in space and time. J Physiol (Lond) 229:1–32.

Eccles JC, Ito M, Szentagothai J (1967) The cerebellum as a neuronal machine. Berlin: Springer.

Egert U, Heck D, Aertsen A (2002) Two-dimensional monitoring of spiking networks in acute brain slices. Exp Brain Res 142:268–274.

Forti L, Cesana E, Mapelli J, D'Angelo E (2006) Ionic mechanisms of autorhythmic firing in cerebellar Golgi cells. J Physiol (Lond) 574:711–729.

Gall D, Prestori F, Sola E, D'Errico A, Roussel C, Forti L, Rossi P, D'Angelo E (2005) Intracellular calcium regulation by burst discharge determines bidirectional long-term synaptic plasticity at the cerebellum input stage. J Neurosci 25:4813–4822.

Garthwaite J, Brodbelt AR (1989) Synaptic activation of *N*-methyl-D-aspartate and non-*N*-methyl-D-aspartate receptors in the mossy fibre pathway in adult and immature rat cerebellar slices. Neuroscience 29:401–412.

Hamann M, Rossi DJ, Attwell D (2002) Tonic and spillover inhibition of granule cells control information flow through cerebellar cortex. Neuron 33:625–633.

Hansel C, Linden DJ, D'Angelo E (2001) Beyond parallel fiber LTD: the diversity of synaptic and non-synaptic plasticity in the cerebellum. Nat Neurosci 4:467–475.

Harvey RJ, Napper RM (1991) Quantitative studies on the mammalian cerebellum. Prog Neurobiol 36:437–463.

Heuschkel MO, Fejtl M, Raggenbass M, Bertrand D, Renaud P (2002) A three-dimensional multi-electrode array for multi-site stimulation and recording in acute brain slices. J Neurosci Methods 114:135–148.

Hubbard JI, Llinas R, Quastel DMJ (1969) Electrophysiological analysis of synaptic transmission. Baltimore: Williams and Wilkins.

Isope P, Barbour B (2002) Properties of unitary granule cell→Purkinje cell synapses in adult rat cerebellar slices. J Neurosci 22:9668–9678.

Jorntell H, Ekerot CF (2002) Reciprocal bidirectional plasticity of parallel fiber receptive fields in cerebellar Purkinje cells and their afferent interneurons. Neuron 34:797–806.

Kohonen T (1984) Self-organization and associative memory. New York: Springer.

Lisman JE (2003) Long-term potentiation: outstanding questions and attempted synthesis. Philos Trans R Soc Lond B Biol Sci 358:829–842.

Lu H, Hartmann MJ, Bower JM (2005) Correlations between Purkinje cell single unit activity and simultaneously recorded field potentials in the immediately underlying granule cell layer. J Neurophysiol 94:1849–1860.

Maffei A, Prestori F, Rossi P, Taglietti V, D'Angelo E (2002) Presynaptic current changes at the mossy fiber-granule cell synapse of cerebellum during LTP. J Neurophysiol 88:627–638.

Mann-Metzer P, Yarom Y (2000) Electrotonic coupling synchronizes interneuron activity in the cerebellar cortex. Prog Brain Res 124:115–122.

Marr D (1969) A theory of the cerebellar cortex. J Physiol (Lond) 202:437–470.

Medina JF, Mauk MD (2000) Computer simulation of cerebellar information processing. Nat Neurosci Rev 3:1205–1211.

Mitchell SJ, Silver RA (2000a) Glutamate spillover suppresses inhibition by activating presynaptic mGluRs. Nature 404:498–502.

Mitchell SJ, Silver RA (2000b) GABA spillover from single inhibitory axons suppresses low-frequency excitatory transmission at the cerebellar glomerulus. J Neurosci 20:8651–8658.

Mitchell SJ, Silver RA (2003) Shunting inhibition modulates neuronal gain during synaptic excitation. Neuron 38:433–445.

Nieus T, Sola E, Mapelli J, Saftenku E, Rossi P, D'Angelo E (2006) LTP regulates burst initiation and frequency at mossy fiber-granule cell synapses of rat cerebellum: experimental observations and theoretical predictions. J Neurophysiol 95:686–699.

Nowak L, Bregestovski P, Ascher P, Herbet A, Prochiantz A (1984) Magnesium gates glutamate-activated channels in mouse central neurones. Nature 307:462–465.

Petersen CCH, Grinvald A, Sakmann B (2003) Spatiotemporal dynamics of sensory responses in layer 2/3 of rat barrel cortex measured *in vivo* by voltage-sensitive dye imaging combined with whole-cell voltage recordings and neuron reconstructions. J Neurosci 23:1298–1309.

Ramon y Cajal S (1911) Histologie du system nerveux de l'homme et des vertebres. Paris: Maloine.

Rieke F, Warland D, de Ruyter van Stevenink R, Bialek W (1997) Spikes. London: MIT.

Schonewille M, Khosrovani S, Winkelman BHJ, Hoebeek FE, De Jeu MTG, Larsen IM, Van Der Burg J, Schmolesky MT, Frens MA, De Zeeuw CI (2006) Purkinje cells in awake behaving animals operate at the upstate membrane potential. Nat Neurosci 9:459–461.

Shambes GM, Gibson JM, Welker W (1978) Fractured somatotopy in granule cell tactile areas of rat cerebellar hemispheres revealed by micromapping. Brain Behav Evol 15:94–140.

Sims RE, Hartell NA (2005) Differences in transmission properties and susceptibility to long-term depression reveal functional specialization of ascending axon and parallel fiber synapses to Purkinje cells. J Neurosci 25:3246–3257.

Singer W (1999) Time as coding space? Curr Opin Neurobiol 9:189–194.

Sola E, Prestori F, Rossi P, Taglietti V, D'Angelo E (2004) Increased neurotransmitter release during long-term potentiation at mossy fibre-granule cell synapses in rat cerebellum. J Physiol (Lond) 557:843–861.

Sultan F (2001) Distribution of mossy fibre rosettes in the cerebellum of cat and mice: evidence for a parasagittal organization at the single fibre level. Eur J Neurosci 13:2123–2130.

von Békésy G (1967) Mach band type lateral inhibition in different sense organs. J Gen Physiol 50:519–532.

Vos BP, Volny-Luraghi A, De Schutter E (1999) Cerebellar Golgi cells in the rat: receptive fields and timing of responses to facial stimulation. Eur J Neurosci 11:2621–2634.

Wirth C, Lüscher H (2004) Spatiotemporal evolution of excitation and inhibition in the rat barrel cortex investigated with multielectrode arrays. J Neurophysiol 91:1635–1647.

Wu HS, Sugihara I, Shinoda Y (1999) Projection patterns of single mossy fibers originating from the lateral reticular nucleus in the rat cerebellar cortex and nuclei. J Comp Neurol 411:97–118.